Separation Science and Technology
Publication details, including instructions for authors and subscription information:
http://www.informaworld.com/smpp/title~content=t713708471

A Numerical Analysis of Surface Diffusion in a Binary Adsorbed Film

G. F. Round[a]; H. W. Habgood[a]; R. Newton[a]
[a] Research Council of Alberta, Edmonton, Alberta

To cite this Article Round, G. F. , Habgood, H. W. and Newton, R.(1966) 'A Numerical Analysis of Surface Diffusion in a Binary Adsorbed Film', Separation Science and Technology, 1: 2, 219 — 244
To link to this Article: DOI: 10.1080/01496396608049446
URL: http://dx.doi.org/10.1080/01496396608049446

SEPARATION SCIENCE, 1(2 & 3), 219–244 (1966)

A Numerical Analysis of Surface Diffusion in a Binary Adsorbed Film*,†

G. F. ROUND, H. W. HABGOOD, and R. NEWTON
RESEARCH COUNCIL OF ALBERTA, EDMONTON, ALBERTA

Summary

Based on the assumptions that the adsorption of a binary gas mixture may be described by Langmuir isotherms and that the rate of diffusion into the interior of the adsorbent is proportional to the gradient in chemical potential, equations are developed to describe the adsorption of a binary mixture by a slab and by a sphere. The equations describing the concentration changes of each component are coupled nonlinear second-order partial differentials and were solved numerically for the following boundary conditions (normalized concentrations θ of the components at the surface): $\theta_A:\theta_B =$ 0.05:0.90, 0.05:0.05, 0.475:0.475, and 0.875:0.095 and ratios of diffusivities, $L_A/L_B = 2$, 10, and 200. Profiles of concentration against distance into a slab or sphere and also curves of total uptake against time (all in dimensionless form) were obtained. The distinctive feature of the results is that the component of higher diffusivity advances ahead of the second component and tends to attain temporary local concentrations much higher than the equilibrium values at the boundary. Consequently, the total uptake of the more-mobile component may pass through a maximum. These effects are most pronounced when the difference in diffusivities is large, when the equilibrium concentration of the component of higher diffusivity is small, and when the total equilibrium concentration of the two components is large. The calculations were applied to previously reported results of the adsorption of nitrogen-methane mixtures by zeolite A and were found to give reasonable correlations between the behavior of mixtures and that of the individual pure components. In the case of near saturation ($\theta_A + \theta_B \rightarrow 1$ at the boundary), the fit with experiment is particularly sensitive to the exact value of $(1 - \theta_A - \theta_B)$.

* Contribution No. 334 from the Research Council of Alberta, Edmonton, Canada.
† Additional information and details relating to this work are deposited with Research Council of Alberta and copies may be obtained on request from the librarian.

Separations using selective adsorption of one component from a mixture usually are based on differences in adsorptive affinity of the various components. These affinities are equilibrium properties and the behavior of a mixture can usually be estimated from a knowledge of the behavior of the individual components. Such is also often the case with molecular-sieve-type adsorbents—here a component may show negligible adsorption, because its molecules are too large to penetrate the fine channels of the adsorbent. The selective adsorption of straight-chain paraffin hydrocarbons from mixtures containing branched-chain and cyclic hydrocarbons by the calcium form of zeolite A (molecular sieve 5A) is a well-known example. Interesting possibilities arise, however, when the molecular-sieve action is incomplete, i.e., when compounds may be adsorbed but at relatively slow rates because of the slow diffusion processes by which they penetrate into the interior of the adsorbent. If the diffusivities of the various components are different from each other, the composition of the adsorbed phase will change with time and a true equilibrium adsorption is obtained only after a long time. Barrer and Robins (*1*) have summarized the various possible combinations that may arise with binary mixtures depending on the relative adsorptivities and diffusivities of the two components. They also list examples for the different situations taken from studies with dehydrated crystalline zeolites which, because of their regular crystal structure, show well-marked molecular-sieve properties.

From the point of view of practical separations, one of the most interesting of the cases listed by Barrer and Robins involves adsorption from a binary mixture in which the component having the greater affinity for the adsorbent is also the more slowly diffusing component. Here it is possible that the component having the lower adsorptivity may yet be preferentially taken up during the early stages of adsorption. An example of such a system previously reported (*2*) from this laboratory is the adsorption of mixtures of nitrogen and methane by the sodium form of zeolite A. Methane is more strongly adsorbed than nitrogen but the rate of diffusion of nitrogen into the crystal is higher than that of methane. In the early stages of adsorption of nitrogen-methane mixtures by outgassed zeolite, nitrogen is preferentially adsorbed, sometimes to such a degree that the amount taken up may temporarily be greater than that corresponding to the final equilibrium adsorption. It is thus possible to selectively remove either nitrogen or methane from

the gas mixture, depending upon whether the process is terminated in a short or a long time. The equilibrium condition achieved at long times and corresponding to preferential adsorption of methane was found to be roughly predictable using a mixed Langmuir isotherm; the transient condition during which nitrogen is preferentially adsorbed depends upon both adsorptivities and diffusivities, and the complex relationships involved are the subject of this present paper.

For such a system the rate-determining steps appear to be the activated diffusion of each species through the regular network of intracrystalline channels of the adsorbent. These channels are windows connecting a regular array of cavities, each large enough to contain several adsorbate molecules. The windows, however, are of such a size that a significant activation energy is required before molecules can pass through. The effective diameter of a nitrogen molecule is smaller than that of a methane molecule, so the activation energy for movement of nitrogen through the crystal of zeolite A is somewhat lower than for methane.

It was suggested that a satisfactory description of this system could be made by assuming diffusion to occur under a gradient in chemical potential, with the equilibrium surface concentrations being described by a Langmuir isotherm. The more usual treatment of diffusion in terms of the gradient in concentration leads to highly variable diffusion coefficients and even to negative coefficients for the "uphill" diffusion that must occur when the nitrogen uptake exceeds its equilibrium value. As pointed out in the previous paper (2), the concept of the gradient in chemical potential as the driving force for diffusion has been used frequently; some authors, most recently Meeks and Beveridge (3), have advocated the gradient in activity as the fundamental driving force.

The present work is a theoretical extension of the earlier experimental study through a numerical analysis of the equations developed for the assumption that the velocity of diffusion is proportional to the gradient in chemical potential. Although conventional experiments give only the total adsorption of a system of particles, the computations show, in addition, the concentration profiles through an individual particle. The results are presented in terms of generalized coordinates for a range of parameters for the two cases of adsorption into an infinite slab and into a sphere, representing experimental cases of diffusion into thin sheets and into particles. Within the range of parameters studied, an approximate

comparison is made with the experimental results of the earlier paper. These calculations are also of interest as being an example of a numerical solution by finite-difference methods of a system of coupled nonlinear second-order partial differential equations.

THEORETICAL

Derivation of the Fundamental Equations

Following the earlier treatment (2), the velocity of diffusion in an adsorbed film is assumed to be proportional to the gradient in the chemical potential,

$$u_A = -L_A \nabla \mu_A \tag{1}$$

where L_A is the proportionality constant and μ_A is the chemical potential of species A. The flux J_A of diffusing material therefore is given by the following equation, which corresponds to Fick's first law:

$$J_A = C_A u_A = -C_A L_A \nabla \mu_A \tag{2}$$

where C_A is the concentration of A. In principle, a second term of the form $C_A L_{AB} \nabla \mu_B$ should also be included, but as a first approach the coefficient L_{AB} is assumed to be zero. From the equation of continuity one obtains

$$\frac{\partial C_A}{\partial t} + \nabla (J_A) = 0 \tag{3}$$

For unidirectional flow in the x direction,

$$\frac{\partial C_A}{\partial t} = \frac{\partial}{\partial x}\left(C_A L_A \frac{\partial \mu_A}{\partial x}\right) \tag{4}$$

corresponding to Fick's second law. A similar equation applies to the second species, B, in a two-component mixture.

To apply these equations to an actual adsorbent-adsorbate system the chemical potential must be related to the concentrations of adsorbate in the adsorbent. If the gas at 1 atm is taken as the standard state, the chemical potential of the adsorbate is given by

$$\mu_A = \mathscr{R}T \ln p_A \tag{5}$$

$$\mu_B = \mathscr{R}T \ln p_B \tag{6}$$

where $p_{A(B)}$ is the partial pressure in atmospheres of gas A(B) in equilibrium with the adsorbed film. For a binary adsorbed film obeying the Langmuir isotherm,

$$p_A = \frac{\theta_A}{b_A(1 - \theta_A - \theta_B)} \tag{7}$$

$$p_B = \frac{\theta_B}{b_B(1 - \theta_A - \theta_B)} \tag{8}$$

where $\theta_A = C_A/C_M$ and $\theta_B = C_B/C_M$. C_M is the adsorbate concentration corresponding to a monolayer coverage, which is assumed the same for both adsorbates. It follows that

$$\frac{\partial p_A}{\partial \theta_A} = \frac{1 - \theta_B}{b_A(1 - \theta_A - \theta_B)^2} \tag{9}$$

$$\frac{\partial p_A}{\partial \theta_B} = \frac{\theta_A}{b_A(1 - \theta_A - \theta_B)^2} \tag{10}$$

Differentiating Eq. (5) with respect to x, we obtain

$$\frac{\partial \mu_A}{\partial x} = \frac{\mathscr{R}T}{p_A}\frac{\partial p_A}{\partial x} = \frac{\mathscr{R}T}{p_A}\left(\frac{\partial p_A}{\partial \theta_A}\frac{\partial \theta_A}{\partial x} + \frac{\partial p_A}{\partial \theta_B}\frac{\partial \theta_B}{\partial x}\right) \tag{11}$$

Substitution of p_A, $\partial p_A/\partial \theta_A$, and $\partial p_A/\partial \theta_B$ from Eqs. (7), (9), and (10), respectively, results in

$$\frac{d\mu_A}{\partial x} = \frac{\mathscr{R}T}{\theta_A(1 - \theta_A - \theta_B)}\left[(1 - \theta_B)\frac{\partial \theta_A}{\partial x} + \theta_A \frac{\partial \theta_B}{\partial x}\right] \tag{12}$$

Substituting this function for $\partial \mu_A/\partial x$ in Eq. (4) and replacing C_A by $\theta_A C_M$ gives

$$\frac{\partial \theta_A}{\partial t} = \frac{\partial}{\partial x}\left\{\frac{\mathscr{R}TL_A}{1 - \theta_A - \theta_B}\left[(1 - \theta_B)\frac{\partial \theta_A}{\partial x} + \theta_A \frac{\partial \theta_B}{\partial x}\right]\right\} \tag{13}$$

or

$$\frac{\partial \theta_A}{\partial t} = \frac{\mathscr{R}TL_A}{1 - \theta_A - \theta_B}\left[(1 - \theta_B)\frac{\partial^2 \theta_A}{\partial x^2} + \theta_A \frac{\partial^2 \theta_B}{\partial x^2}\right] + \frac{\mathscr{R}TL_A}{(1 - \theta_A - \theta_B)^2}\left[(1 - \theta_B)\frac{\partial \theta_A}{\partial x} + \theta_A \frac{\partial \theta_B}{\partial x}\right]\left(\frac{\partial \theta_A}{\partial x} + \frac{\partial \theta_B}{\partial x}\right) \tag{14}$$

and similarly for component B,

$$\frac{\partial\theta_B}{\partial t}=\frac{\mathscr{R}TL_B}{1-\theta_A-\theta_B}\left[(1-\theta_A)\frac{\partial^2\theta_B}{\partial x^2}+\theta_B\frac{\partial^2\theta_A}{\partial x^2}\right]$$
$$+\frac{\mathscr{R}TL_B}{(1-\theta_A-\theta_D)^2}\left[(1-\theta_A)\frac{\partial\theta_B}{\partial x}+\theta_B\frac{\partial\theta_A}{\partial x}\right]\left(\frac{\partial\theta_B}{\partial x}+\frac{\partial\theta_A}{\partial x}\right) \quad (15)$$

In the limiting case of the diffusion of a single component at low concentration, Eq. (14) reduces to the usual expression of Fick's second law with a Fick diffusion coefficient equal to $\mathscr{R}TL_A$.

Finite-difference forms of Eqs. (14) and (15) were developed (see the next section) to describe the diffusional behavior of a binary-gas mixture in an adsorbed film for the one-dimensional case, i.e., diffusion into an infinite plane slab.

The same theory can be generalized for three-dimensional diffusion for which the equation corresponding to (14) expressed in vector notation is

$$\frac{\partial\theta_A}{\partial t}=\frac{\mathscr{R}TL_A}{1-\theta_A-\theta_B}\left[(1-\theta_B)\nabla^2\theta_A+\theta_A\nabla^2\theta_B\right]$$
$$+\frac{\mathscr{R}TL_A}{(1+\theta_A-\theta_B)^2}\left[(1-\theta_B)|\nabla\theta_A|^2+\theta_A|\nabla\theta_B|^2\right.$$
$$\left.+(1+\theta_A-\theta_B)(\nabla\theta_A)\cdot(\nabla\theta_B)\right] \quad (16)$$

For uniform spherical diffusion, $\theta_A=\theta_A(t, r)$, so $\nabla\theta_A=(\partial\theta_A/\partial r)i$ (gradient of θ_A) and $\nabla^2\theta_A=(\partial^2\theta_A/\partial r^2)+[(2/r)(\partial\theta_A/\partial r)]$ and Eq. (16) takes the form

$$\frac{\partial\theta_A}{\partial t}=\frac{\mathscr{R}TL_A}{1-\theta_A-\theta_B}\left[(1-\theta_B)\left(\frac{\partial^2\theta_A}{\partial r^2}+\frac{2}{r}\frac{\partial\theta_A}{\partial r}\right)+\theta_A\left(\frac{\partial^2\theta_B}{\partial r^2}+\frac{2}{r}\frac{\partial\theta_B}{\partial r}\right)\right]$$
$$+\frac{\mathscr{R}TL_A}{(1-\theta_A-\theta_B)^2}\left[(1-\theta_B)\frac{\partial\theta_A}{\partial r}+\theta_A\frac{\partial\theta_B}{\partial r}\right]\left(\frac{\partial\theta_A}{\partial r}+\frac{\partial\theta_B}{\partial r}\right) \quad (17)$$

for component A and

$$\frac{\partial\theta_B}{\partial t}=\frac{\mathscr{R}TL_B}{1-\theta_A-\theta_B}\left[(1-\theta_A)\left(\frac{\partial^2\theta_B}{\partial r}+\frac{2}{r}\frac{\partial\theta_B}{\partial r}\right)+\theta_B\left(\frac{\partial^2\theta_A}{\partial r}+\frac{2}{r}\frac{\partial\theta_A}{\partial r}\right)\right]$$
$$+\frac{\mathscr{R}TL_B}{(1-\theta_A-\theta_B)^2}\left[(1-\theta_A)\frac{\partial\theta_B}{\partial r}+\theta_B\frac{\partial\theta_A}{\partial r}\right]\left(\frac{\partial\theta_B}{\partial r}+\frac{\partial\theta_A}{\partial r}\right) \quad (18)$$

for component B. As described later, it was found necessary for reasons of the stability of some of the numerical computations to

carry out a transformation of the independent variable and to rewrite Eqs. (17) and (18) in terms of the variable $U = 1/r$, giving

$$\frac{\partial\theta_A}{\partial t} = \frac{\mathscr{R}TL_AU^4}{1-\theta_A-\theta_B}\left\{(1-\theta_B)\frac{\partial^2\theta_A}{\partial U^2} + \theta_A\frac{\partial^2\theta_B}{\partial U^2} + \frac{1}{1-\theta_A-\theta_B}\left[(1-\theta_B)\frac{\partial\theta_A}{\partial U} + \theta_A\frac{\partial\theta_B}{\partial U}\right]\left(\frac{\partial\theta_A}{\partial U} + \frac{\partial\theta_B}{\partial U}\right)\right\} \quad (19)$$

$$\frac{\partial\theta_B}{\partial t} = \frac{\mathscr{R}TL_BU^4}{1-\theta_A-\theta_B}\left\{(1-\theta_A)\frac{\partial^2\theta_B}{\partial U^2} + \theta_B\frac{\partial^2\theta_A}{\partial U^2} + \frac{1}{1-\theta_A-\theta_B}\left[(1-\theta_A)\frac{\partial\theta_B}{\partial U} + \theta_B\frac{\partial\theta_A}{\partial U}\right]\left(\frac{\partial\theta_A}{\partial U} + \frac{\partial\theta_B}{\partial U}\right)\right\} \quad (20)$$

Equations (17) and (18) or (19) and (20) were developed as finite-difference equations for the numerical calculation of diffusion into a sphere.*

Finite-Difference Equations for Determination of Concentration Profiles

Equations (14), (15), (17), (18), (19), and (20) were written in explicit forward-marching finite-difference form (*4*) as follows:

(*a*) *Infinite plane slab.* Diffusion into an infinite plane slab assuming equal concentrations of each component on each side of the slab leads to a symmetric distribution of material about the center plane of the slab. To describe this slab for the purpose of computation, a mesh system in time and space was applied, with equal time increments Δt and equal space increments Δx. A concentration $\theta(t, x)$ is then approximated by that at the nearest mesh point $(i\,\Delta t, j\,\Delta x)$ and the continuous function $\theta(t, x)$ is replaced by a finite number of values $\theta(i, j)$, for $i \geq 0$ and $j = 1, \ldots, N$; $i = 0$ is the starting time of the experiment, $j = 1$ is the center of the slab, and $j = N$ is the surface of the slab.

The first and second space derivatives were used in central difference form:

$$\left(\frac{\partial\theta_A}{\partial x}\right)_{i,j} = \frac{\theta_A(i, j+1) - \theta_A(i, j-1)}{2\,\Delta x} \quad (21)$$

$$\left(\frac{\partial^2\theta_A}{\partial x^2}\right)_{i,j} = \frac{\theta_A(i, j+1) + \theta_A(i, j-1) - 2\,\theta_A(i, j)}{(\Delta x)^2} \quad (22)$$

* The corresponding equations for diffusion into a cylinder of finite length are derived and included in the deposited material.

where i is a time variable and j a space variable. The mesh is of constant spacing Δx, so for a plane sheet successive increments in thickness correspond to equal increments in volume. The time derivative was expressed as a forward difference,

$$\left(\frac{\partial \theta_A}{\partial t}\right)_{i,j} = \frac{\theta_A(i+1, j) - \theta_A(i, j)}{\Delta t} \tag{23}$$

The center of the slab is a plane of symmetry for the concentration of profiles. Thus, at this point $(\partial\theta_A/\partial x)_{i,1} = 0$, and Eq. (22) for the center point becomes

$$\left(\frac{\partial^2 \theta_A}{\partial x^2}\right)_{i,1} = \frac{2[\theta_A(i, 2) - \theta_A(i, 1)]}{(\Delta x)^2} \tag{24}$$

Substituting Eqs. (21) to (23) in (14) and (15) gives the complete finite-difference equations for an infinite plane slab at the point (i, j) representing the increments in concentration at that point over the increase in time from $i\,\Delta t$ to $(i + 1)\,\Delta t$:

$$\begin{aligned}\theta_A(i+1, j) = A_x\{&(1 - \theta_B(i, j))D_2\theta_A + \theta_A(i, j)D_2\theta_B \\ &+ [(1 - \theta_B(i, j))D\theta_A + \theta_A(i, j)D\theta_B] \\ &\times [D\theta_A + D\theta_B]/[1 - \theta_A(i, j) - \theta_B(i, j)]\}/[1 \\ &- \theta_A(i, j) - \theta_B(i, j)] + \theta_A(i, j)\end{aligned} \tag{25}$$

$$\begin{aligned}\theta_B(i+1, j) = B_x\{&(1 - \theta_A(i, j))D_2\theta_B + \theta_B(i, j)D_2\theta_A \\ &+ [(1 - \theta_A(i, j))D\theta_B + \theta_B(i, j)D\theta_A] \\ &\times [D\theta_B + D\theta_A]/[1 - \theta_A(i, j) - \theta_B(i, j)]\}/[1 \\ &- \theta_A(i, j) - \theta_B(i, j)] + \theta_B(i, j)\end{aligned} \tag{26}$$

where $A_x = \mathscr{R}TL_A\,\Delta T/(\Delta x)^2$, $B_x = \mathscr{R}TL_B\,\Delta T/(\Delta x)^2$, and the abbreviations $D_2\theta_A$ and $D\theta_A$ are used for the differences,

$$\begin{aligned}D_2\theta_A &= \theta_A(i, j+1) + \theta_A(i, j-1) - 2\theta_A(i, j) \\ D\theta_A &= (\theta_A(i, j+1) - \theta_A(i, j-1))/2\end{aligned}$$

with similar definitions for $D_2\theta_B$ and $D\theta_B$.

(*b*) *Sphere.* Several sets of calculations were made for a given set of boundary conditions; these involved the space derivatives in various forms. The time derivative was put into forward-difference, forward-marching, explicit form—as in Eq. (22). The space derivatives were put into differing forms, using both constant and variable mesh sizes (5), and using both central- and forward-difference approximations. For a sphere the assigned mesh system corresponded to a series of spherical surfaces at $r = r_j$ for $j = 1$,

. . . , N, where $r_1 = 0$ is the center and r_N is the outer surface of the sphere. The space derivatives of the concentrations $\left(\frac{\partial\theta}{\partial r}\right)_{i,j}$ and $\left(\frac{\partial^2\theta}{\partial r^2}\right)_{i,j}$ at a point (i, j) in time and space are then given by

$$\left(\frac{\partial\theta}{\partial r}\right)_{i,j} = \frac{\theta_A(i, j+1)(\Delta r_{j-1})^2 - \theta_A(i, j-1)(\Delta r_j)^2 - \theta_A(i, j)[(\Delta r_{j-1})^2 - (\Delta r_j)^2]}{\Delta r_j\, \Delta r_{j-1}(\Delta r_j + \Delta r_{j-1})} \quad (27)$$

$$\left(\frac{\partial^2\theta}{\partial r^2}\right)_{i,j} = \frac{\theta_A(i, j+1)\, \Delta r_{j-1} + \theta_A(i, j-1)\, \Delta r_j - \theta_A(i, j)(\Delta r_{j-1} + \Delta r_j)}{0.5\, \Delta r_j\, \Delta r_{j-1}(\Delta r_j + \Delta r_{j-1})} \quad (28)$$

where $\Delta r_j = r_{j+1} - r_j$ for $r = 1, \ldots, N-1$. Again, i and j refer to time and space variables, respectively.

The finite-difference forms referred to in the above equations were obtained by truncating Taylor-series expansions of the functions at the appropriate point. The central-difference forms are accurate to the order of Δ^2, and the forward-difference forms not given but used in some calculations are accurate to the order of Δ.

Equal radial increments in the case of a sphere mean unequal volume increments. Calculations were made with two types of spacing, constant mesh size and variable mesh size, giving constant volume increments of the sphere. In the latter case, the necessary values of Δr_j in Eqs. (27) and (28) were calculated from

$$\frac{4}{3}\pi(r_{j+1}^3 - r_j^3) = \frac{4\pi r_N^3}{3(N-1)} \quad (29)$$

Once the number of increments had been decided, the values of the radii and hence Δr_j were calculated.

In the case of constant mesh size, the volume increment V_j is given by

$$V_j = \frac{4}{3}\pi(j^3 - (j-1)^3)\left(\frac{r_N}{N-1}\right)^3 \quad (30)$$

At the center of the sphere $(\partial\theta/\partial r) = 0$ and $r = 0$, so the terms $(2/r)(\partial\theta_A/\partial r)$ and $(2/r)(\partial\theta_B/\partial r)$ are indeterminate as such. However, writing a Taylor-series expansion of $\partial\theta/\partial r$ about the center gives

$$\frac{\partial\theta(t, \Delta r)}{\partial r} = \frac{\partial\theta(t, 0)}{\partial r} + \Delta r\, \frac{\partial^2\theta(t, 0)}{\partial r^2} + \cdots$$

Hence in the limit as $\Delta r \rightarrow 0$, $(1/\Delta r)[\partial\theta(dr)/\partial r]$ becomes $\partial^2\theta/\partial r^2$ at the center. Therefore, in Eqs. (17) and (18), $(\partial^2\theta_A/\partial r^2) + [(2/r)(\partial\theta_A/\partial r)]$ was replaced by $3(\partial^2\theta_A/\partial r^2)$ and $(\partial^2\theta_B/\partial r^2) + [(2/r)(\partial\theta_B/\partial r)]$ was replaced by $3(\partial^2\theta_B/\partial r^2)$ at $j = 1$.

The finite-difference forms of the equations for diffusion into a sphere, corresponding to Eqs. (25) and (26) for diffusion into a slab, follow in an equally straightforward manner from Eqs. (17) and (18) and from (19) and (20) and are not given in detail.

The calculation of concentration profiles within the slab or sphere may be made for successive times from given initial concentration profiles by use of the finite-difference equations and appropriate values of the constants L_A, L_B, and T and of the dimensions of the slab or sphere, $X(=x_N)$ or $R(=r_N)$, respectively. The results of such calculations, however, are of greatest general utility when expressed in generalized dimensionless form, and this has been done in the calculations of this paper. The concentrations θ are already dimensionless in the preceding equations. Distances were made dimensionless by normalizing to the half-thickness of the slab, X, or the radius of the sphere, R, and expressed as $\bar{x} = x/X$ and $\bar{r} = r/R$. A dimensionless time was introduced by the relations

$$\tau = \frac{\mathscr{R}TL_A t}{X^2} \quad \text{or} \quad \tau = \frac{\mathscr{R}TL_A t}{R^2} \tag{31}$$

In terms of the quantities actually used in the calculations, the dimensionless time of Eq. (31) was expressed in slightly different forms for the two cases of constant mesh-size spacing and variable mesh-size spacing. For constant mesh-size spacing,

$$\tau = \frac{n}{(N-1)^2} A_{x(r)} \tag{32}$$

where n = number of time increments
$N - 1$ = number of mesh increments
$A_{x(r)} = \mathscr{R}TL_A\ \Delta t/(\Delta x)^2$ or $\mathscr{R}TL_A\ \Delta t/(\Delta r)^2$

For a variable mesh-size spacing the quantity $\mathscr{R}TL_A/\ \Delta t/R^2$ was treated as a constant in the calculations so that $\tau = n\mathscr{R}TL_A\ \Delta t/R^2$.

Determination of Total Uptake by Integration of Concentration-Distance Profiles

In many experimental situations the quantities of principal interest are the total amounts of the two components that are ad-

sorbed at any one time. The total uptake of material is determined by appropriate integration of the concentration profile over the thickness of the slab or the radius of the sphere. To obtain these integrals in the present calculations, a trapezoidal summation was used and the total quantities adsorbed, Q, were expressed in normalized form relative to the maximum capacity of the slab or sphere (i.e., $Q = 1$ for $\theta = 1$ throughout the structure).

Choice of Mesh for Calculations of Spherical Diffusion

As indicated previously, calculations for binary diffusion into a sphere were carried out using two types of mesh spacing: a constant mesh spacing and one corresponding to equal increments of volume. A number of exploratory calculations were carried out to investigate the effects of changes in the type of mesh, in the number of mesh increments, in the method of calculating differences, and (see the following section) in the magnitude of the time increment.

The effects of different mesh systems may be assessed most readily from an examination of the curves of uptake against square root of time; for any diffusion process these plots are expected to be initially linear from the origin. Figure 1 shows a number of such plots for diffusion into a sphere with a ratio of constants $A_r/B_r = L_A/L_B = 200$ and surface boundary conditions of $\theta_A = 0.05$ and $\theta_B = 0.90$. Constant spacing of 10 equal increments using forward-difference and central-difference forms together with variable spacing (equal volumes) of 10 and 20 increments decreasing in size from the center of the sphere to the surface were investigated. Curves I and II, which were obtained using a mesh of constant spacing, are concave upward at small times. The values obtained for component A appear to be too small and the values for component B too large, so the curves for B appear to intersect the Q axis at a significant positive value. Apart from the error introduced from the finite-difference approximation, the major error arises from the integration by the trapezoidal rule. In a short time component A reaches a maximum concentration near the surface of the sphere (see Fig. 3); the concentration curve is markedly peaked within a distance of one or two mesh increments and trapezoidal integration is least accurate here. In addition, from Eq. (30) it can be seen that the increments close to the surface represent concentric spheres of greater volume than increments close to the

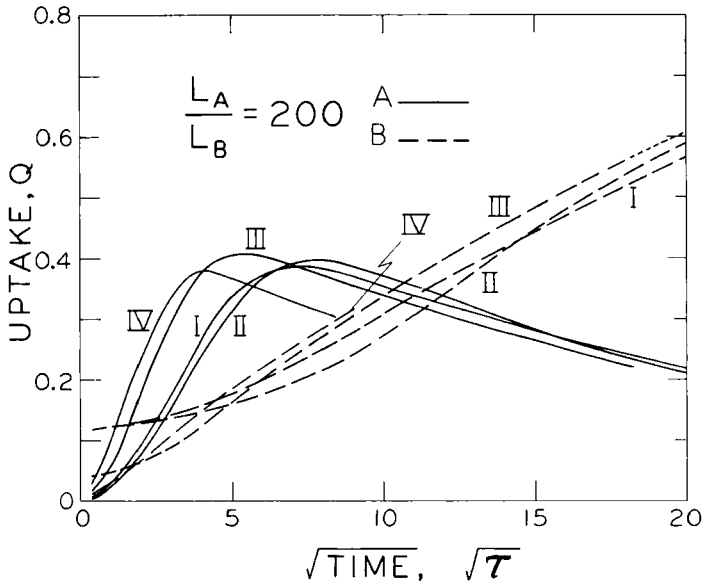

FIG. 1. Effect of mesh size and mesh spacing on curves of uptake against square root of time (both quantities in dimensionless form) for diffusion into a sphere, $\theta_A = 0.05$, $\theta_B = 0.90$ at the surface, $L_A/L_B = 200$. I, 10 equal intervals forward differences; II, 10 equal intervals, central differences; III, variable spacing, 10 intervals, central differences; IV, variable spacing, 20 intervals, central differences.

center of the sphere. Thus any error which results in poor resolution in increments close to the surface is *additionally magnified* in the calculation of the total uptake. A trapezoidal summation tends to underestimate the uptake of A in the region of the maximum in concentration and to overestimate the uptake of B, for which the concentration profile is curved in the opposite sense. The calculations in this instance show little distinction between the use of forward differences (curve I) and central differences (curve II) in the first derivatives, although the latter form is more accurate.

The use of a variable mesh with the same number of spaces leads to a significant improvement (curve III). The concavity of the curve for component A is decreased, probably because of better resolution of the maximum in the concentration curve, so the value of the summation becomes larger. For the same reason the curve for component B more nearly extrapolates to the origin.

The use of a decreased mesh size should lead to better resolution of the concentration profiles and hence to a more reliable determination of the amount adsorbed. Curves IV in Fig. 1, based on a variable mesh of 20 increments, show significant improvement in linearity at small times. To reduce computation times and to get a wider range of results for a qualitative comparison it was considered more practical to use a 10-increment, variable-size mesh. But for the quantitative comparisons a 20-increment system was used.

Diffusion into a plane slab does not involve such errors; equal space increments give equal volume increments, and no additional magnification of the error is involved in summation because of unequal volumes.

Stability

Approximating a partial differential equation with a finite-difference equation introduces errors into its solution, the size of which are determined by the $\Delta(x, r)$, Δt, and the degree of the approximation. These errors are propagated in both the time and space dimensions, and for a valid solution it is necessary that this propagation does not result in a significant accumulation of error with the increase in calculation. Otherwise the calculations will eventually accumulate errors larger than the solution values, and the system is then termed unstable. In simpler systems of equations it is possible to assume a random error and to determine the limits of Δx, etc., for which the solutions are stable, but for the present system it was necessary to determine the limits by experiment.

It was decided that a reasonable mesh spacing from the point of view of resolution and computation time would be 10 spaces and the majority of computations have been made with this number. The constants in the equations $A_{x(r)}$, $B_{x(r)}$ were chosen for their largest value while maintaining a stable solution. This meant that the value of Δt was made as large as possible.* For example, with a 10-space mesh, an infinite slab with $L_A/L_B = 200$ and $\theta_A = 0.05$, $\theta_B = 0.90$ could be solved with $A_x = 0.1$ and $B_x = 0.0005$ ($A_x/B_x = 200$); for $L_A/L_B = 2$, the values of A_x and B_x were 0.05 and 0.025.

* The work of Funk and Houghton (6) on the solution of two coupled nonlinear partial differential equations indicated that the optimum Δt should be the maximum allowable for stability.

Coefficients greater than these caused the solutions to become unstable.

The first differential in a second-order differential equation is a frequent source of instability in its finite-difference form. When, as in the case of spherical diffusion, the combination $(1/r)(\partial\theta/\partial r)$ occurs, the error is magnified as $r \rightarrow 0$. Thus the solution becomes unstable for relatively smaller time increments than is possible in the case of slab diffusion. The transformation $U = 1/r$ eliminates the $(1/r)(\partial\theta/\partial r)$ terms [Eqs. (20) and (21)], and combined with the variable-mesh-size system these factors produced stability for practical time increments which otherwise was not found possible for $L_A/L_B < 200$. This transformation was used for all calculations of diffusion into a sphere with variable mesh size.

RESULTS AND DISCUSSION

Calculations were carried out using a 20K IBM 1620 digital computer.* In all cases component A was taken to be the component with higher diffusivity; the ratio of diffusivity of the two components, L_A/L_B, was varied between 2 and 200. The boundary condition of near saturation, $\theta_A + \theta_B = 0.95$, was considered to represent the situation of greatest interest, in which competition of the two species for the available surface would be high. The different situations investigated are summarized in Table 1 and selected results are given in the figures.

The Effect of the L_A/L_B Ratio

The primary effect of an increase in the L_A/L_B ratio shows the expected behavior of the faster-moving species A, advancing ahead of B into the empty adsorbent and approaching local concentrations corresponding to the adsorption of A alone at the same partial pressure. The extent to which A is able to advance ahead of B and achieve its temporary high concentration is dependent upon the relative diffusion coefficients. Figures 2 and 3 show concentration profiles for L_A/L_B ratios of 2 and 200 for diffusion into a sheet and into a sphere under boundary conditions of $\theta_A = 0.05$ and $\theta_B = 0.90$. The values of dimensionless time τ, corresponding to each curve, are all comparable and are proportional to the real diffusion time

* The computer programs written in FORTRAN, together with selected results for all cases of Table 1, are included in the material that has been deposited.

TABLE 1
Summary of Numerical Investigations

	Boundary conditions				Relative diffusivities	Mesh size No. of Δx or Δr
	θ_A	θ_B	$\theta_A + \theta_B$	θ_A/θ_B	L_A/L_B	center to surface
			Diffusion into a Plane Sheet			
1	0.05	0.90	0.95	18	2	10
2	0.05	0.90	0.95	18	10	10
3	0.05	0.90	0.95	18	200	10
4	0.475	0.475	0.95	1	2	10
5	0.855	0.095	0.95	0.11	2	10
			Diffusion into a Sphere			
6	0.05	0.90	0.95	18	2	10
7	0.05	0.90	0.95	18	10	10
8[a]	0.05	0.90	0.95	18	200	10
9	0.05	0.90	0.95	18	200	20
10	0.05	0.05	0.10	1	2	10
11	0.475	0.475	0.95	1	2	10
12	0.855	0.095	0.95	0.11	2	10

[a] Using the conditions set out in 8, several investigations were made on the effect of different forms of the first derivative, e.g., as forward and central differences using a mesh of constant spacing, i.e., unequal volume increments.

for the A component. Thus in a comparison of the curves for ratios of 2 and 200, component A may be considered to represent the same substance in each case, whereas component B refers to substances having diffusivities $\frac{1}{2}$ and $\frac{1}{200}$ that of A. The lower the diffusivity of B (e.g., $L_A/L_B = 200$), the more chance A has to build up to a maximum concentration ahead of B.

The curves of total uptake, Figs. 4 and 5, show the increasing temporary advantage for component A as L_B decreases. These curves refer to the case where B is the major component at equilibrium and as the diffusivity of B decreases, component A has a longer time to accumulate ahead of B. Consequently, the maximum in A is greater and is attained at a greater time.

The differences between planar flow and spherical flow are perhaps best seen by comparing Figs. 4 and 5. Diffusion into the center of a sphere compared with a plane, for the same L_A/L_B ratio, is much more rapid, as a result of converging flux lines for the sphere. It is interesting to note that the maximum concentration of A for a given diffusion ratio is approximately the same for planar and spherical

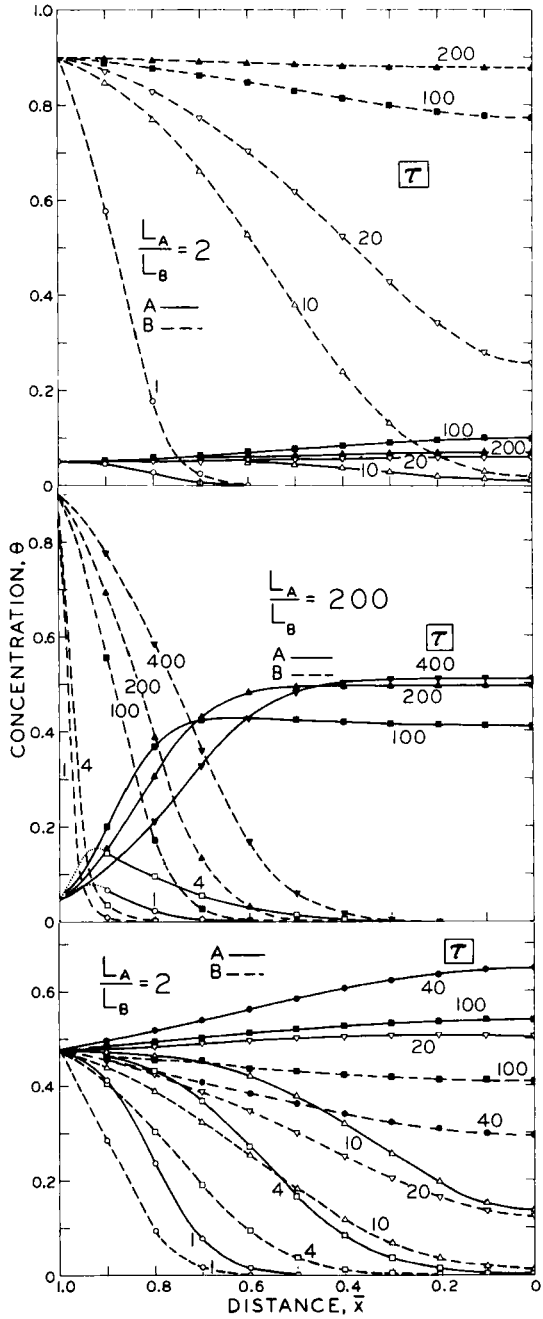

FIG. 2. Binary diffusion into an infinite plane slab. Concentration-distance profiles for various values of dimensionless time, τ. Boundary conditions (concentrations at external surface of slab) held constant at values shown for $\bar{x} = 1$. Relative diffusivities, L_A/L_B, as indicated. Calculations using a uniform mesh of 10 intervals with central differences.

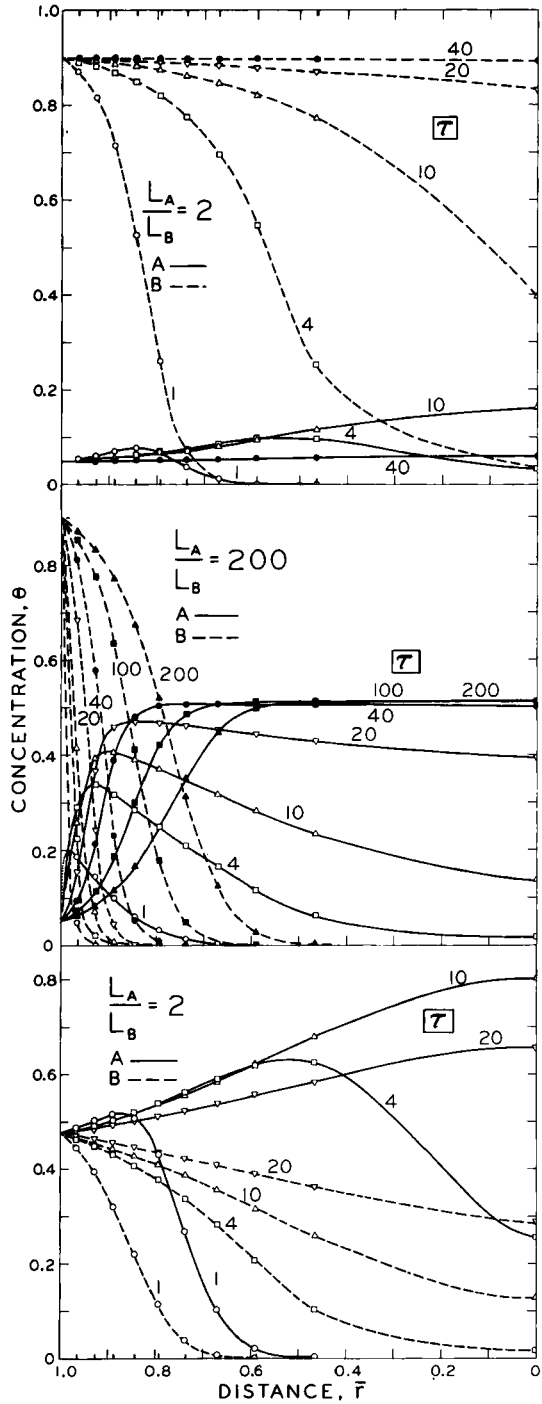

FIG. 3. Binary diffusion into a sphere. Concentration-distance profiles for various values of dimensionless time, τ. Boundary conditions (concentrations at external surface) held constant at values shown for $\bar{r} = 1$. Relative diffusivities, L_A/L_B, as indicated.

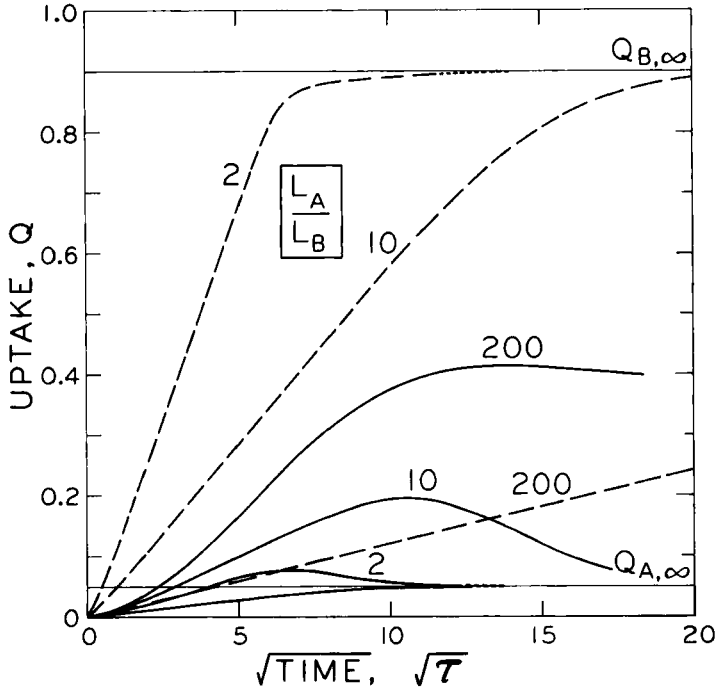

FIG. 4. Binary diffusion into a plane slab, uptake against square root of time (dimensionless). Boundary values $\theta_A = 0.05$; $\theta_B = 0.90$; relative diffusivities L_A/L_B as indicated. The lowermost curve is for the uptake of A alone from a boundary condition $\theta_A = 0.05$.

flow. Figure 6 shows a comparison between flow into a plane slab and a sphere for $L_A/L_B = 200$ and boundary concentrations of $\theta_A = 0.05$ and $\theta_B = 0.90$ in both cases. The maximum concentration of component A for the spherical case is achieved in about a quarter of the time taken for the planar case.

The relative diffusivity of the more rapid component A has little effect on the uptake of the slower component B, particularly when the slower component is the more strongly retained at equilibrium. This is seen in Fig. 7, which shows the uptake of B in the presence of different A components of diffusivities 2 and 200 times that of B.

The Effect of Boundary Conditions

Figures 8 and 9 show that the temporary maximum in A relative to the equilibrium value is larger when A is the minor component

at equilibrium and when the total surface coverage at equilibrium is high. It is interesting, however, that a slight maximum in A is observed even when A is the major component ($\theta_A = 0.855$ and $\theta_B = 0.095$). In case II of Fig. 9, corresponding to equilibrium concentrations of each component of 0.05, the maximum in A has disappeared. A comparison of Figs. 8 and 9 shows that the time scale for spherical flow as noted before is, in effect, contracted in comparison to planar flow; the maxima in amounts adsorbed occur earlier in Fig. 9 than in Fig. 8. The magnitude of the peaks is much the same. In addition, the final equilibrium condition is achieved in the same time for all the boundary conditions for one type of diffusion. For the plane this occurs at $\tau^{1/2} \sim 1.5$, for the sphere, at $\tau^{1/2} \sim 0.7$.

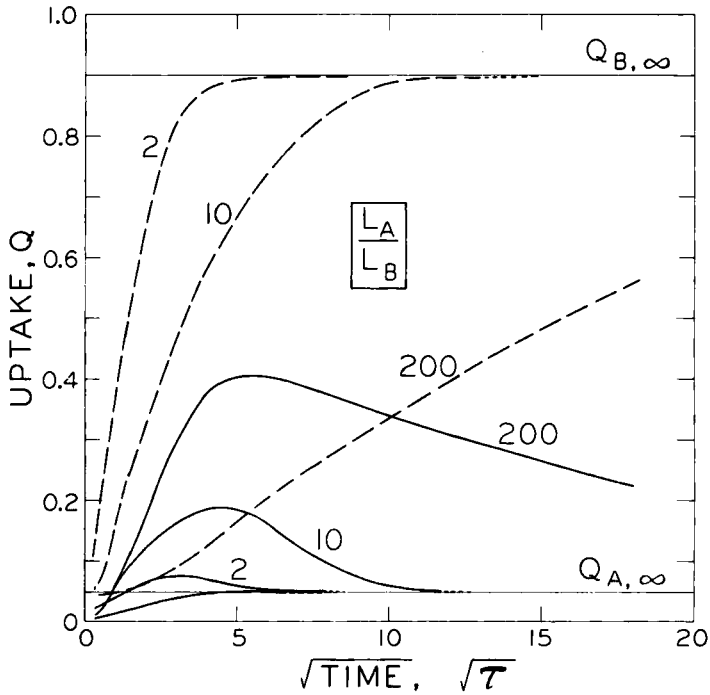

FIG. 5. Binary diffusion into a sphere, uptake against square root of time (dimensionless). Boundary values, $\theta_A = 0.05$, $\theta_B = 0.90$; relative diffusivities L_A/L_B as indicated. The lowermost curve is for the uptake of A alone from a boundary condition of $\theta_A = 0.05$.

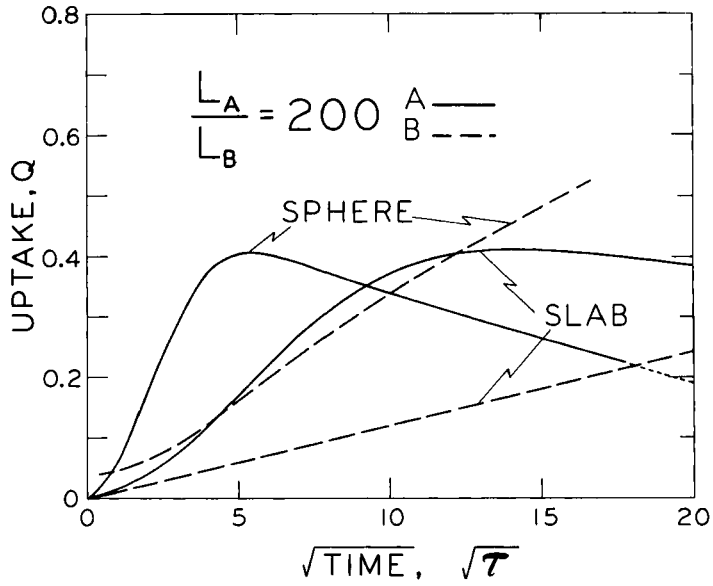

FIG. 6. Comparison of uptake by a slab and by a sphere; boundary conditions $\theta_A = 0.05$, $\theta_B = 0.90$; $L_A/L_B = 200$.

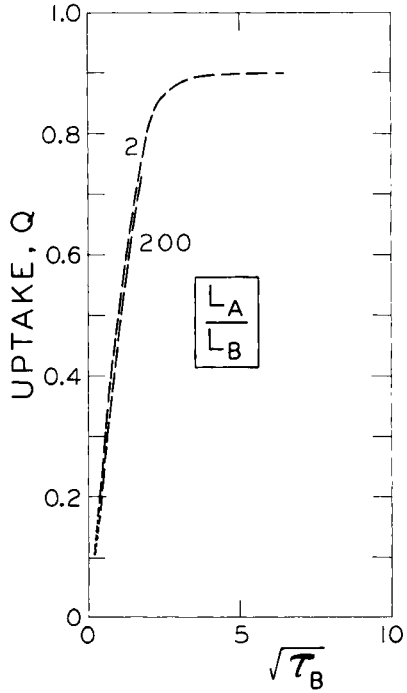

FIG. 7. Effect of component A on the uptake of B. Diffusion into a sphere, $\theta_A = 0.05$, $\theta_B = 0.90$ at the surface; $L_A/L_B = 2$, 200. The time scale for these curves is $(\tau_B)^{1/2}$ in which B_r is substituted for A_r in the expression of Eq. (30).

Comparison with Experiment

The mathematical model proposed in this paper may be used to predict sorption behavior for comparison with previously published experimental results for the sorption of nitrogen-methane mixtures by molecular sieve 4A (*1*). The most complete set of experimental data refer to a sample of the zeolite powder activated at 400°C. Table 2 lists the monolayer capacities and the diffusion coefficients for the uptake of the individual pure gases at two temperatures. Using these values, the curves of uptake were calculated for the four situations included in Fig. 5 of (*1*): sorption from 10% and from 50% gaseous nitrogen-methane mixtures at 0 and −79°C. The boundary values, θ, were taken as the experimentally observed limiting equilibrium values of the uptake expressed as fractions of the monolayer capacities. The agreement with experiment was good

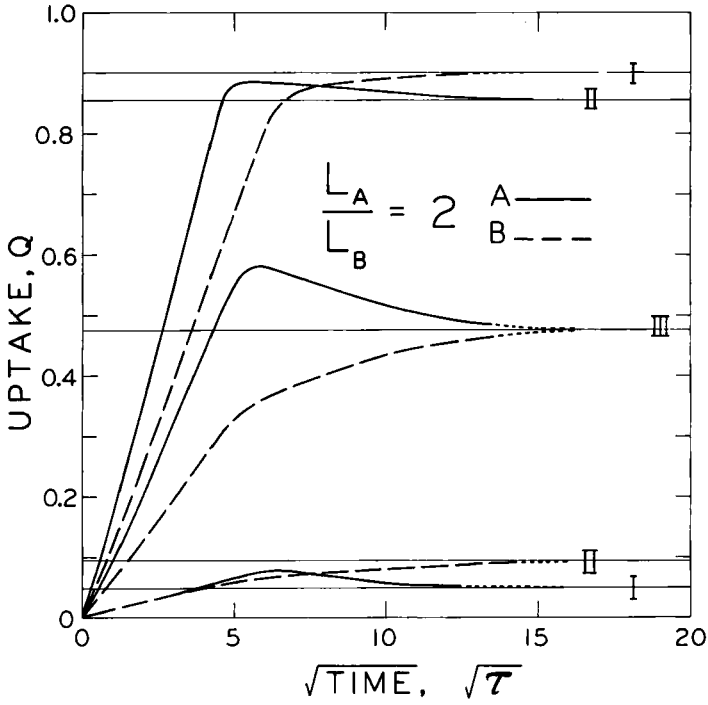

FIG. 8. Binary diffusion into a plane slab. Uptake against square root of time (dimensionless). $L_A/L_B = 2$. Effect of various boundary concentrations: Curve I: θ_A, 005; θ_B, 0.90. Curve II: θ_A, 0.855; $\theta_B = 0.095$. Curve III: $\theta_A = 0.475$; $\theta_B = 0.475$.

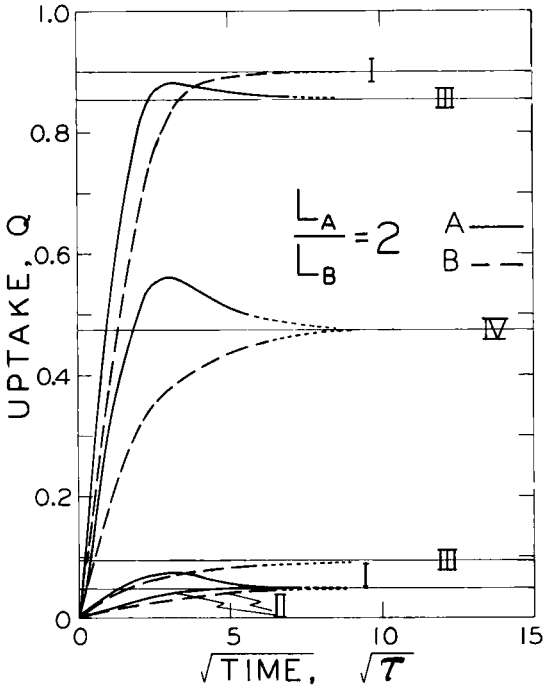

FIG. 9. Binary diffusion into a sphere, uptake against square root of time (dimensionless). $L_A/L_B = 200$. Effect of various boundary conditions: Curve I: $\theta_A = 0.05$; $\theta_B = 0.90$. Curve II: $\theta_A = 0.05$; $\theta_B = 0.05$. Curve III: $\theta_A = 0.855$; $\theta_B = 0.095$. Curve IV: $\theta_A = 0.475$; $\theta_B = 0.475$.

for the measurements made at 0°C, where the sum of the uptakes of the two gases was less than one quarter of the monolayer capacity of the zeolite, but was quantitatively rather poor for the measurements at −79°C, where the total uptake was over 98% of the monolayer capacity. The comparison is given in parts (a) and (b) of Fig. 10 for two cases that illustrate these situations. Normalized uptake, Q, is plotted against the square root of real time. The calculated curves were determined using the L_A and τ/t values of Table 2 and the boundary conditions calculated from the average monolayer capacities: θ_{N_2} and θ_{CH_4} of 0.015 and 0.238 for 10% N_2 at 0°C; 0.063 and 0.921 for 10% N_2 at −79°C. A variable-size mesh of 20 intervals was used in the calculations.

The rather poor fit between the calculated and experimental

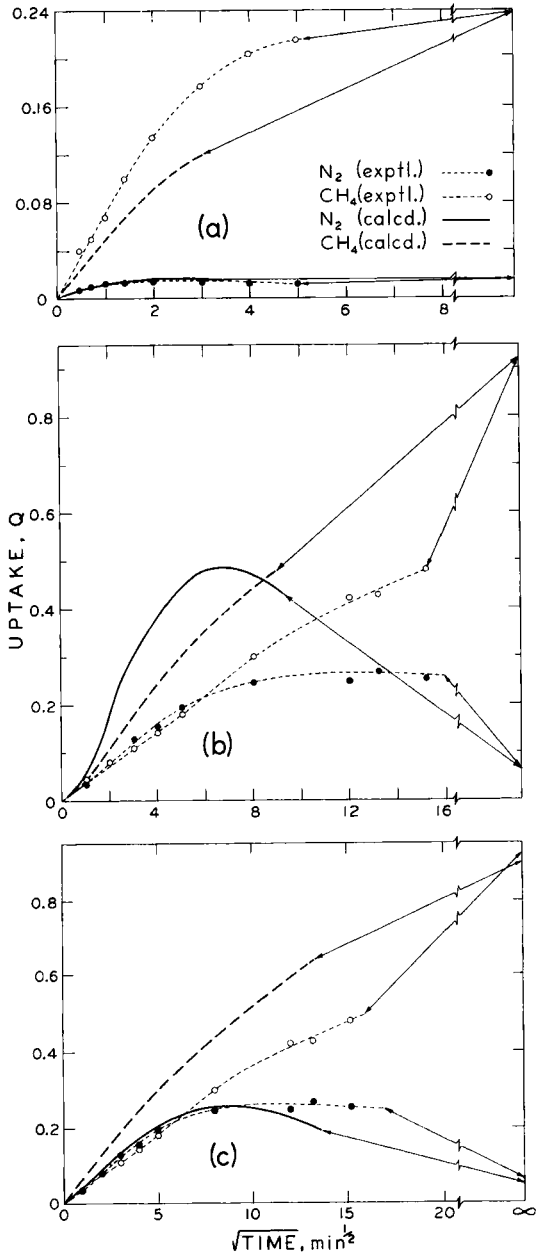

FIG. 10. Comparison of calculated uptakes for a sphere with experimental values (2) for adsorption of N_2-CH_4 mixtures by zeolite A powder. (a) Adsorption from 10% N_2 (in gas phase) at 0°C, 1 atm. Boundary conditions $\theta_{N_2} = 0.015$, $\theta_{CH_4} = 0.238$; $L_{N_2}/L_{CH_4} = 16.4$. (b) Adsorption from 10% N_2 (in gas phase) at −79°C, 1 atm. Boundary conditions $\theta_{N_2} = 0.063$, $\theta_{CH_4} = 0.921$; $L_{N_2}/L_{CH_4} = 21.8$. (c) Experimental values of (b) compared with calculated curves for boundary conditions, $\theta_{N_2} = 0.05$, $\theta_{CH_4} = 0.90$; $L_{N_2}/L_{CH_4} = 25$.

TABLE 2

Sorption of Nitrogen and Methane by Molecular Sieve 4A (2)
(Powder Activated at 400°C; Mean Particle Radius = 2.5×10^{-5} cm)

Temp., °C	Langmuir monolayer, C_M, ml(STP)/g			Diffusion coefficient, $\mathscr{R}TL$, cm²/sec			$\tau/t = \mathscr{R}TL_A/R^2$, sec⁻¹
	N_2	CH_4	Av.	N_2	CH_4	L_{N_2}/L_{CH_4}	
0	86.8	104.0	95.4	1.29×10^{-12}	7.87×10^{-10}	16.4	2.06×10^{-3}
−79	77.2	79.5	78.4	3.42×10^{-14}	1.37×10^{-13}	21.8	5.47×10^{-5}

values in Fig. 10 (b) probably is related to the great sensitivity of the calculations to the factor $1/(1 - \theta_A - \theta_B)$, which increases rapidly as $(\theta_A + \theta_B) \rightarrow 1$. For example, a decrease of only 3% in $(\theta_A + \theta_B)$ from the value 0.984 used in the calculations to 0.95 means a decrease in $1/(1 - \theta_A - \theta_B)$ from 62.5 to 20—a change of 200%. Consideration of the data of (2) suggests that the values of C_M used to determine the θ's could easily be uncertain by such an amount; the isotherm measurements were taken considerably below saturation, and although the Langmuir equation was a reasonable fit to these data, some departure at high coverages would not be unexpected. Furthermore, different monolayer capacities resulted for the two adsorbates, although the theory requires only a single value. The curves in Fig. 10 (c) illustrate the considerable improvement in agreement with experiment obtained by taking boundary conditions of $\theta_A = 0.05$ and $\theta_B = 0.90$, giving a total $(\theta_A + \theta_B) = 0.95$. The curves were calculated for the slightly different ratio $L_A/L_B = 25$ instead of 21.8, but the additional effect of this change is minor. In view of the limitations of the model, particularly concerning the quantitative application of the Langmuir isotherm, any further adjustment of parameters is not warranted.

We feel that, on the whole, the model discussed in this paper gives a satisfactory description of binary adsorption by zeolites, in which the rate of adsorption is governed by activated surface diffusion. The temporary maximum in the uptake of the more rapidly diffusing species is clearly shown. The behavior near saturation is sensitive to the precise form of the adsorption isotherm, and it is possible that an extension of this approach to other systems might require a modification of the development to incorporate some other form of adsorption isotherm. The good agreement between the calculated and experimental values of the uptake of each

component gives confidence that the calculated concentration profiles (which are inherently difficult or impossible to measure) may also be reasonable.

Nomenclature

A, B	constants for a given mesh system
b	constant in Langmuir equation
C	concentration of adsorbed material
i, j	mesh points i (time), j (space)
J	flux of sorbed material
L	proportionality constant in diffusion equation
N	number of mesh points
n	number of time increments
p	partial pressure
$\mathscr{R}$	gas constant
R	r_N = radius of sphere
r	distance from surface of sphere
$\bar{r}$	r/R
T	absolute temperature
t	time
V	volume
X	x_N = slab half-thickness
x	distance from center to surface of a plane infinite slab
$\bar{x}$	x/X
$\Delta r, \Delta x$	space increments for sphere and plane infinite sheet
Δt	time increments
θ	ratio of concentration of adsorbate in structure to adsorbate concentration in monolayer
μ	chemical potential of adsorbate relative to pure gas at 1 atm and same temperature

Subscripts

A	component A
B	component B
i, j	mesh points i (time), j (space)
M	monolayer coverage of surface
N	number of locations
r	referring to sphere
x	referring to slab

REFERENCES

1. R. M. Barrer and A. R. Robins, *Trans. Faraday Soc.*, **49**, 807 (1953).
2. H. W. Habgood, *Can. J. Chem.*, **36**, 1384 (1958).
3. F. R. Meeks and D. L. Beveridge, paper presented to the 144th Meeting of the American Chemical Society, Los Angeles, April 1963.
4. R. D. Richtmyer, *Difference Methods for Initial-Value Problems*, Wiley-Interscience, New York, 1958, Chap. 6.
5. G. F. Round, R. Newton, and P. J. Redberger, *Chem. Eng. Progr. Symp. Ser.*, **58**, 29 (1962).
6. J. E. Funk and G. Houghton, *J. Chromatog.*, **6**, 193 (1961).

Received by editor February 3, 1966
Submitted for publication April 25, 1966